

Fluid mechanics of lean blowout precursors in gas turbine combustors

T. M. Muruganandam¹ and J. M. Seitzman²

¹Assistant Professor, Aerospace Engineering Department, Indian Institute of Technology Madras, Chennai, India

²Professor, School of Aerospace Engineering, Georgia Institute of Technology, Atlanta, Georgia, USA.

Received April 10, 2011; Accepted April 19, 2011

ABSTRACT

Understanding of lean blowout (LBO) phenomenon, along with the sensing and control strategies could enable the gas turbine combustor designers to design combustors with wider operability regimes. Sensing of precursor events (temporary extinction-reignition events) based on chemiluminescence emissions from the combustor, assessing the proximity to LBO and using that data for control of LBO has already been achieved. This work describes the fluid mechanic details of the precursor dynamics and the blowout process based on detailed analysis of near blowout flame behavior, using simultaneous chemiluminescence and droplet scatter observations. The droplet scatter method represents the regions of cold reactants and thus help track unburnt mixtures. During a precursor event, it was observed that the flow pattern changes significantly with a large region of unburnt mixture in the combustor, which subsequently vanishes when a double/single helical vortex structure brings back the hot products back to the inlet of the combustor. This helical pattern is shown to be the characteristic of the next stable mode of flame in the longer combustor, stabilized by double helical vortex breakdown (VBD) mode. It is proposed that random heat release fluctuations near blowout causes VBD based stabilization to shift VBD modes, causing the observed precursor dynamics in the combustor. A complete description of the evolution of flame near the blowout limit is presented. The description is consistent with all the earlier observations by the authors about precursor and blowout events.

1. INTRODUCTION

Increasingly stringent emissions standards have directed many current efforts to improve power and propulsion systems towards clean, environmentally friendly power generation. Improvements focus on reducing pollutant emissions, while improving efficiency and lowering costs without significant change in reliability. In order to

*Corresponding author: E-mail: murgji@iitm.ac.in

achieve low NO_x emissions from gas turbine engines, there has been growing interest in fuel lean premixed combustors. In both premixed and partially premixed combustors, however, the risk of flame blowout increases as the mixture is made leaner, because the weaker combustion process is more vulnerable to small perturbations in combustor conditions [1, 2]. Lean blowout (LBO) poses a problem in both steady and transient situations, e.g., when rapid power changes are required, for both aircraft and land-based turbine engine combustors. Lean blowout in an aircraft engine poses an especially significant safety hazard for example, during power reductions involved in approach and landing. Currently stable performance is ensured by operating the combustor with a wide margin above the uncertain LBO limit. Enhanced performance will require a reduction of this LBO margin. This requires understanding the behavior of the flame very close to blowout.

There have been studies to understand the actual cause of extinction of simple flames. Several researchers have studied the cause of extinction in stagnation plane flames and concluded that strain rate is an important cause [3, 4]. There is evidence that local extinction of the flame is related to the magnitude and the rate of change of the local instantaneous strain rate [5]. Turbulent counterflow flames can exist even past the extinction strain rate for short duration depending on its history of strain [6, 7]. It was found that the flame weakened gradually with periodic forcing of the flame, and thus extinction occurred after several cycles of forcing.

There have been very few studies on blowout phenomena in practical combustors. A number of specific characteristics of flame behavior associated with lean flame stability have been studied by researchers. For example, Nicholson and Field [8] observed large scale pulsations in the flame as it was blowing off. They also reported that the main flame detached and reattached to the flame holder before extinguishing completely. Chao *et al.* [9] observed similar phenomenon in a non-premixed, turbulent jet flame during the blowout process. They reported that prior to blowout, the flame alternated between attachment and detachment to the burner lip. They also noted that this process can last a few short cycles or up to several seconds. Hedman *et al.* [10] imaged the OH radical distribution in a premixed natural gas/air combustor using PLIF. They observed significant flame instability near lean blowout and noted that there was a significant amount of time when there was essentially no OH present in the combustor. Other researchers have also observed fluctuations or transient behavior very close to blow out [11–16]. Thus it is evident that the flame goes through large scale unsteadiness in reacting zone and heat release during the transition process from stable combustion to blowout. There have been several numerical studies that simulate the nonlinear dynamics before the LBO limit in simple combustors [17–19]. They show that apparently chaotic combustion can occur near the extinction limit if full interaction of the fluid dynamics and the transport process are taken into account [20]. There is also a recent analytical work that shows that the combustor is exponentially more susceptible to disturbances as LBO limit is approached [21]. They also predict that the frequency of oscillations is very low and of the order of 15–25 Hz and these oscillations were linked to chaotic behavior of the combustor.

Similar, (but non-periodic) unsteady events have been identified, from both chemiluminescence and acoustic radiation, as precursors to LBO in an atmospheric pressure swirl-dump combustor. In fact, their rate of occurrence has been used to sense the proximity to LBO, [22, 23] and a control system based on sensing these precursors was used to avoid blowout by active control of fuel distribution in the combustor [24, 25]. In those works, the physics of the flow was not clear as to how the phenomenon occurs and why the particular redistribution of fuel in the combustor worked. Understanding of the loss of stabilization can help in several ways: help advancing the scientific understanding of the dynamics of blowout process, improving the data processing methodology to detect blowout proximity, better placement of the detectors, provide clues on better alternate stabilization mechanisms, and design of combustors with better stabilizations. Our previous work [26] was a first step into understanding the dynamics of these precursor events and the physics that control their characteristics. This work is a more detailed study of the physics and an attempt to explain the previous observations of blowout dynamics from a physical perspective.

2. BACKGROUND

Gas turbine combustors commonly employ swirl and sudden expansion to stabilize the flame. The presence of sufficient swirl causes a toroidal vortex breakdown (VBD) to form in the middle of the combustor (denoted in Figure 3 as the inner recirculation zone, IRZ). There is, in addition, an outer recirculation zone (ORZ) created by the sudden expansion. The presence of the swirl-induced vortex core is suppressed by combustion and the sudden expansion, which makes the inner recirculation zone (IRZ) smaller for the case with combustion [27, 28]. It is also observed that the turbulence characteristics are affected by the combustion process. The turbulent kinetic energy and the velocity fluctuations are increased substantially as a consequence of combustion [29]. It was shown that the formation of large VBD structure in the combustor helps in increasing the fuel consumption rates and thus helps in stabilization of the flame in the combustor [30]. In swirling flows with heat release, it was shown that heat release can drive the flow towards VBD and there could be a subcritical/ transcritical bifurcation depending upon the heat release rate [31]. It was shown that the VBD was an important part of the stabilization mechanism for swirl dump stabilized flame [32]. The vortex breakdown location was controlled in order to control the instability in gas turbine engine combustion [33].

Flow physicists have been studying vortex breakdown phenomenon in swirling flows over several decades [34–37]. Vortex breakdown is observed when there is an adverse pressure gradient in the axis of the flow and the point of breakdown is determined by the strength of swirl, the Reynolds number and the pressure gradient. There are several vortex breakdown (VBD) modes (See Figure 1) that have been observed including bubble and helical types, depending on swirl strength and Reynolds number [35, 38].

The VBD modes can change from one to other depending on the disturbances and swirl strength. A schematic of this transition is shown in Figure 2 adopted from the

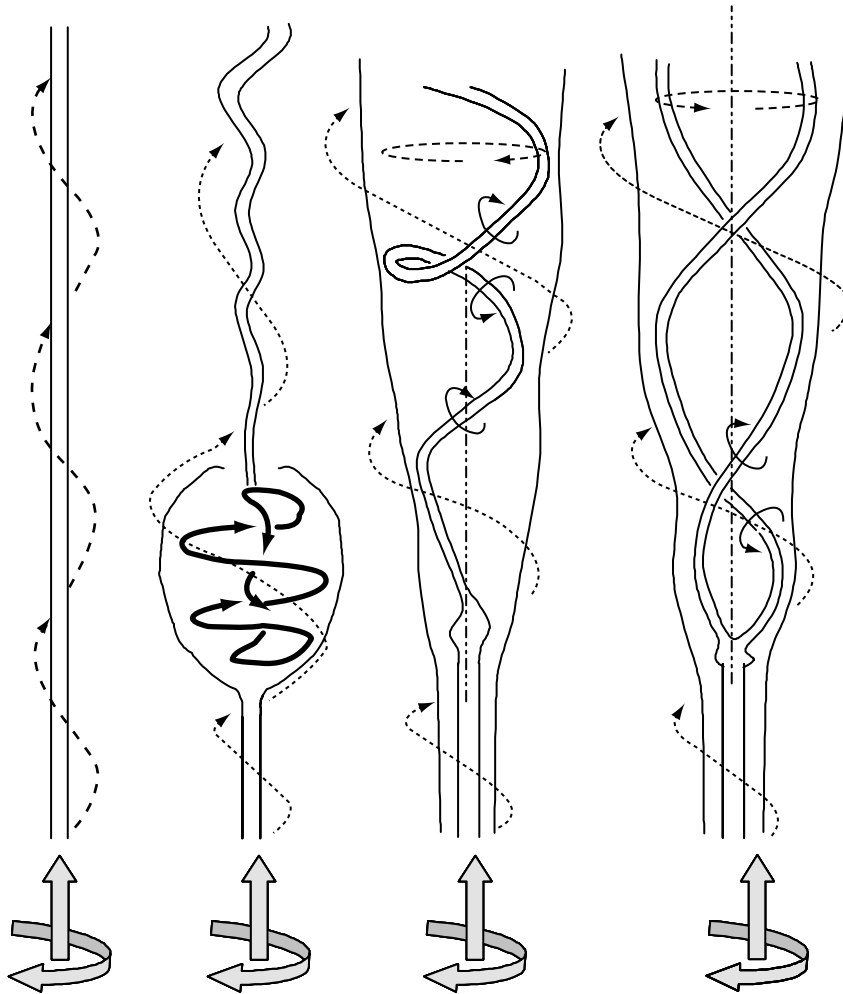


Figure 1: Schematic of the vortex breakdown modes. Left to right: No breakdown, Bubble type breakdown, Single Helical breakdown and Double Helical breakdown. Re and Swirl numbers increase from left to right.

review by Althaus and Weimer [39]. The bubble just becomes weak in structure and unwinds into a helical structure which eventually stabilizes into a helical VBD. In case of formation of the Bubble VBD, there appears a radial transfer of particles which then wraps around itself causing the recirculation structure which eventually rolls up into a bubble VBD. Disturbance which decreases the transfer of axial momentum to radial momentum leads to bubble VBD becoming helical VBD mode and the converse is true of the axial transfer [40].

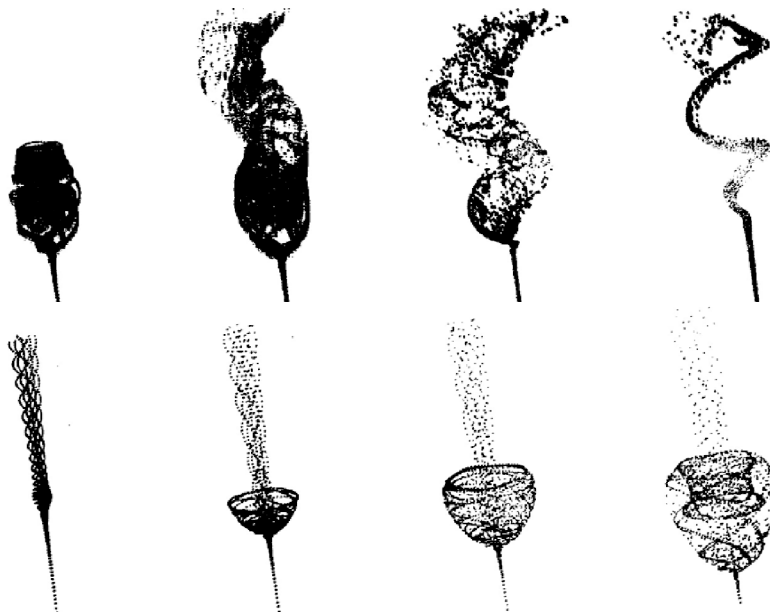


Figure 2: Schematic of transition of vortex breakdown modes. Top: Bubble to spiral, Bottom: Formation of bubble breakdown. Picture adopted from Althaus and Weimer [39].

3. EXPERIMENTAL SETUP

The experiments were performed in an atmospheric pressure, premixed, swirl-stabilized dump combustor. The overall combustor configuration was chosen as a simplified model of a lean, premixed, gas turbine combustor that includes a swirling inlet section. The combustor consisted of an aluminum plate and a quartz tube as shown in Figure 3. The premixed mixture enters the combustor through annular passage between a 1" tube and a 1/4" tube. There are two stages of swirlers 30° and 45° to effect a swirl number of around 0.66. The central tube also carried part of the fuel and air in redistribution studies, depending on the control commands. The current work did not have any flow through the central tube. The combustor walls side wall was made of Quartz tube of 70 mm diameter and 5" long. Experiments were also conducted with a longer tube combustor (8" long). The bottom wall to hold the glass tube was made with aluminum plate. Both the combustors have the same set of stabilization options for the flame, viz., IRZ, ORZ, the jet shear layers and the hot walls.

To help understand the dynamics of the precursor events, a high-speed intensified Videoscope International, Ultracam3 camera was employed. The movie was recorded at 1930 Hz with exposure time of 180 μ sec. Simultaneously, the OH chemiluminescence from the combustor was also collected by a fiber optic probe (a 365 μ m diameter fused

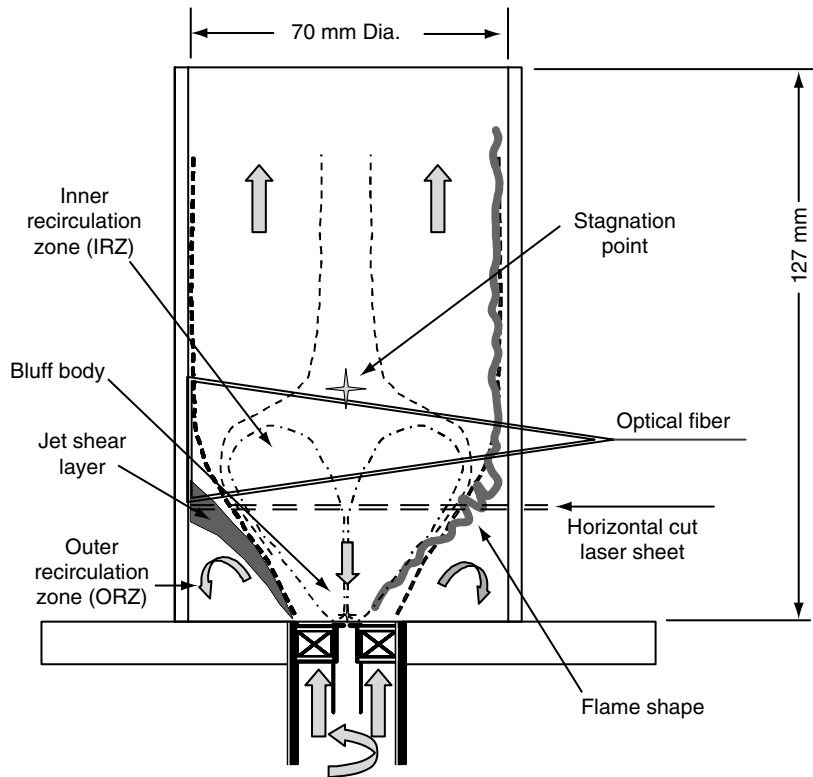


Figure 3: Schematic of the combustor, with flow features, fiber optic collection volume and flame shown.

silica optical fiber) with collection cone half angle of 12° . The collected radiation passes through an interference filter, centered at 308 nm and with a full-width-half-maximum (FWHM) of 10 nm, which corresponds to the primary spectral region for the OH $A^2\Sigma-X^2\Pi$ electronic transition. The collected OH emission is detected by a miniature, metal package PMT (Hamamatsu H5784-04). This PMT has a built-in amplifier (bandwidth of 20 kHz) to convert the current to voltage.

Experiments were also conducted with Olive oil droplet seeded flow. The air stream was seeded with olive oil droplets using a Laskin nozzle [41] based droplet seeder. The seeding system had two nozzle assemblies with four holes of 1 mm diameter. The seed droplets produced are less than $1.2 \mu\text{m}$ in diameter [41] and thus can follow the flow with a frequency response of 10 kHz [42]. A part of the airflow was sent through the seeder and was mixed with the rest of the air before premixing with the fuel. The droplets were illuminated by a 510 nm wavelength laser sheet formed from a copper vapor laser (Metalaser Technologies, Inc, MLT-20). The laser was operated at 5.7 kHz with a 5 W average power ($< 1 \text{ mJ} / \text{pulse}$), and the laser sheet was 89 mm (3.5") in height. In the

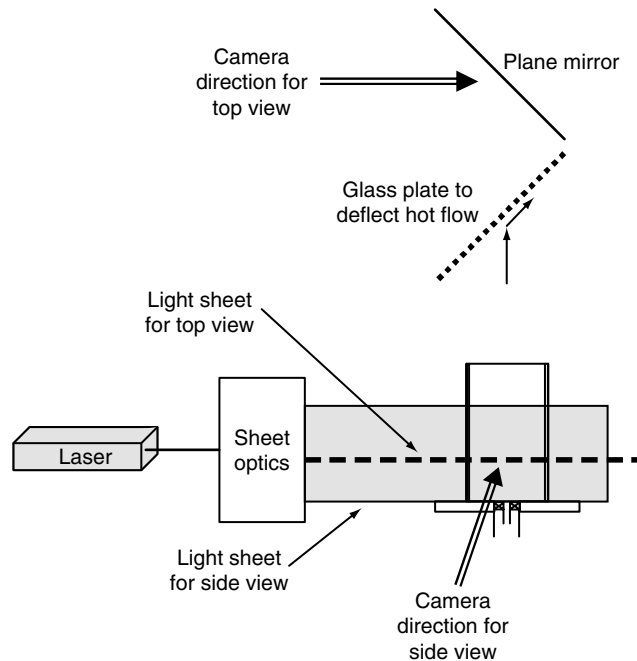


Figure 4: Schematic of the optical setup used to study the combustor in side view and top view. Experiments were not conducted simultaneously as there was only one camera.

droplet scattering experiments, a 510 nm bandpass interference filter (10 nm FWHM) was placed in front of the camera to remove the flame emission, and the camera was triggered once every three laser pulses (at 1.9 kHz) with a gate duration of 60 nsec.

Two laser sheet arrangements were used: vertical sheet (for side view) which covered the bottom 3" of the combustor and the horizontal sheet (for top view) located 1" above the dump plane, as shown in the Figure 4. The top view experiments were conducted with a deflector glass plate to deflect the flow and then a mirror to reflect the light from the droplets into the camera. Again, simultaneous chemiluminescence data from fiber probe was obtained in order to correlate the droplet data with chemiluminescence data.

4. RESULTS AND DISCUSSION

Several modes of flame shapes have been observed in premixed swirl dump combustors. Time-averaged flame shapes are illustrated in Figure 5. The flame shape in conditions closer to LBO limit of the combustor surrounds the IRZ and extends all the way downstream along the wall which we refer to as a V-flame. The flame in the short (5" long) combustor blows off below a certain LBO limit. There is also another shape of the flame in a longer (8" long) combustor for equivalence ratios lower than this LBO

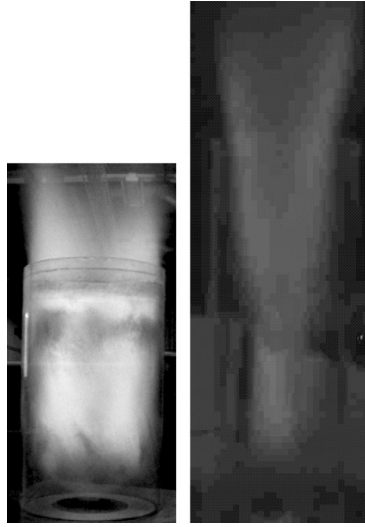


Figure 5: Time averaged photograph of the flame in the combustor for (a) regular combustion ('V-flame') in short tube, and (b) for lower equivalence ratios in longer combustor ('tornado flame').

limit for the short combustor. This flame is weak and has the shape of a tornado funnel (see figure 5) and will be referred to as a tornado flame. If the combustor is not long enough the tornado flame is not stable and the flame blows out. The combustor length of 5" was chosen based on visual observations that this combustor blows off after V-flame suddenly, compared to longer combustors which transitioned into a tornado flame, which lasted even at lower equivalence ratios.

Figure 6 shows the time series data obtained from the optical fiber based OH chemiluminescence sensor. The first and the third rows show data for two different equivalence ratio conditions. The former had an equivalence ratio 0.05 above LBO, at which the combustor has a flame without blowout for a long time. The latter was at the LBO limit, and it can be seen that the combustor blows out after around 10.6 seconds. Expanded views at selected time periods are shown in the second and the fourth rows. The straight horizontal lines are the time averages over 10 seconds of the signal level for comparison. Expanded view of the signal shows that combustion is highly turbulent and packets of burning gases cross the collection volume at random times with random intensities around a mean. The mean value for the higher equivalence ratio is higher than that for the lower equivalence ratio, as expected from heat release point of view. The deviation from mean appears to be the same for both the conditions. There appears, once in a while, a relatively longer absence of flame packet in the collection volume (at 1.05 sec), immediately followed by a bright flame and regular combustion is restored. There are a few long excursions from the mean, towards zero, where the flame has very low signal for extended periods of time, as in 10.9 sec. These events were found to be

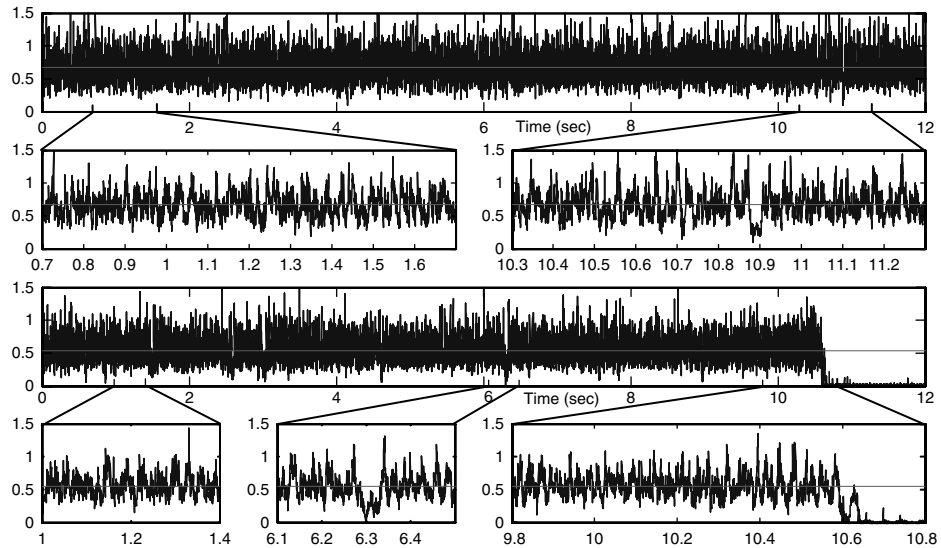


Figure 6: Typical time series variation of local OH chemiluminescence signal for $\phi = 0.77$ (row 1) and $\phi = 0.73$ (row 3), along with a few expanded time series (rows 2 & 4). The straight horizontal lines are averaged signal over first 10 seconds.

the precursor events to blowout, in our previous works. It was shown that they occur only near LBO of this combustor and they occur longer, more in number and occur at random times, as LBO limit is approached. They were used for detection of approach of LBO and control of LBO.

In the case where the combustor is approaching LBO, it can be seen that the deviations towards zero are more in number and longer in duration, compared to a more stable condition. Even at the blowout limit there are times when the combustion resembles regular combustion as shown in the first expanded view in row 4. The second expanded signal shows a precursor event, which is a local extinction followed by reignition of the flame. Comparing this event with the expanded event in the previous signal, one can observe that this event is longer and is more close to zero. Looking at the signal in the third row, it can be seen that there are more excursions towards zero in the condition close to LBO limit. It is also evident that the final LBO event is having the similar rate of extinction as that of the precursor events.

Figure 7 shows the inverted gray scale images of the flame from a single run of the combustor at constant equivalence ratio (at LBO limit). This particular experiment was performed by running the combustor at a slightly higher equivalence ratio for a few seconds and then decreasing the equivalence ratio to the critical value for LBO at fixed air flow rate. This ensures that the walls are heated and will let the flame stay stable for a few seconds without absorbing heat and quenching the flame. The LBO limit fiber

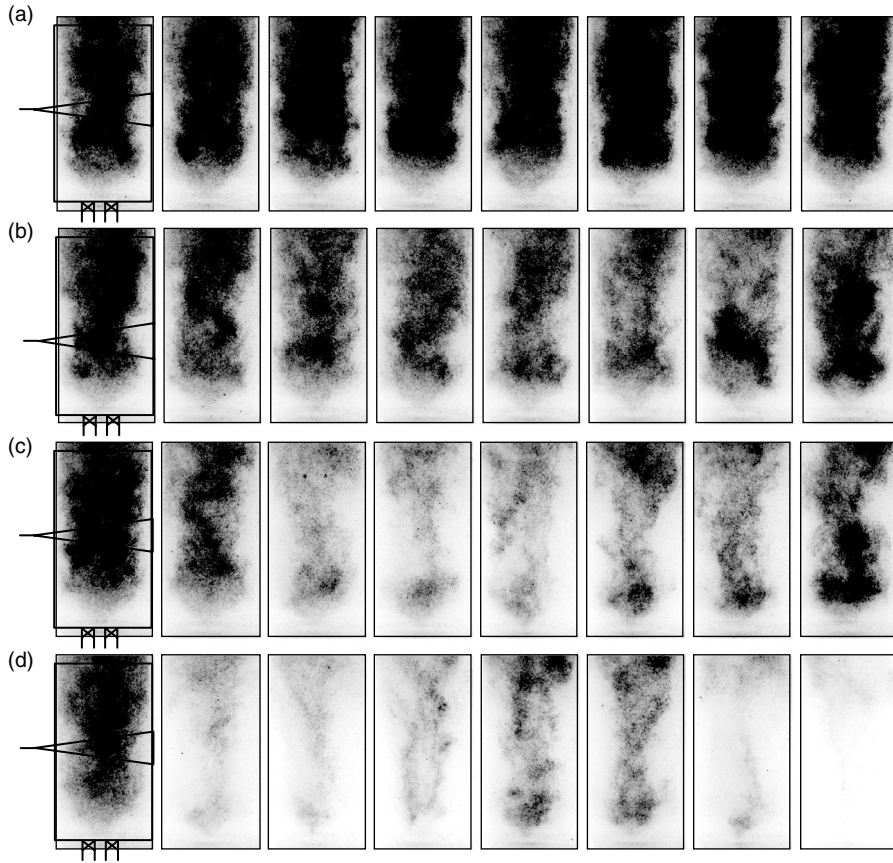


Figure 7: Inverted gray scale movie frames from OH* chemiluminescence emission. (a) regular combustion, (b) a partial precursor event, (c) a precursor event, and (d) a blowout event. All these frames are from the same run with constant flow rate conditions. The image separation for the rows are roughly 2, 2, 4, and 8 msec respectively. The fiber collection volume and the combustor outline are superimposed on the first image in each row.

optic signal presented above was obtained simultaneously with the chemiluminescence movie from which these images were obtained. All the images shown are from the same movie at different time instances.

Figure 7(a) shows a sequence where there is regular combustion, similar to slightly higher equivalence ratios. This is characterized by the flame occupying most of the combustor volume, and the IRZ is very bright. But when closer to blowout, once in a while there are small lapses in the regular combustion, as shown in Figure 7(b). This is characterized by IRZ and the region above becoming less bright and subsequently

returning to regular combustion. Further closer to blowout, these dull flame regions grow in size as shown in Figure 7(c) and occupy a major portion of the combustor.

These events are characterized by local extinction of the flame, followed by a movement of flame from exit upstream towards the inlet which restores flame to regular combustion (V- flame), similar to that in Figure 5(a). Note that images are not having equal separation across rows. These events grow in duration and frequency as the combustor goes closer to LBO. When the combustor blows out, the same event of local extinction occurs, but the flame that comes downwards becomes very weak that it fails to restore the regular combustion and this leads to loss of regular combustion. The general behavior described above is repeatable in almost all the runs conducted in our studies. This sequence is shown in Figure 7(d). Since the flames are weaker, and the flame shape and structure appears to change, a closer analysis is required to understand the extinction-reignition events and blowout event.

Figure 8 shows expanded version of the same extinction-reignition event as in Figure 7(c), with every frame of the movie shown. The first image in this sequence is the same as the second one in Figure 7(c). Note that these images have been multiplied by a factor to increase contrast. One can note that the IRZ and the downstream are becoming weaker in the first row of Figure 8. This is the extinction phase of the precursor event. One can make out the swirling double helical structure of the flame in the rows 2–4. One can also notice that packets of bright flame are moving upstream along the helix occasionally, as marked by the circles. This suggests that the flame packets are moving upstream through rotating helical structures to reach the IRZ. There are two such events occurring in the precursor event as shown in Figure 8. The second flame packet moving to the swirler appears to be more intense, and it manages to restore the IRZ, which now grows in size and intensity. The region above the IRZ is now having more intense flame, while the double helical structure is lost and the regular flame structure as shown in Figure 7(a) is restored.

The frame rate was calculated such that the synchronizing of the frames with the data acquisition was easy and also to ensure that any movement at high speed was also taken care of. The maximum expected velocity in the combustor is 65 m/s near the inlet. The frame rate was 1950 fps to give frame to frame timing of 0.513 msec, during which the gas can move a maximum of 33 mm, which is roughly half the width of the combustor. Thus any movement in the images can be directly used to calculate the velocity of the individual blobs of flame. Quick calculations can show that the vertical component velocity of the flame packets moving downwards are 17.5 and 22 m/s. Since this velocity could not be directly due to turbulent flame going against flow, there has to be a reverse flow field in this helical VBD structure. There were velocity measurements in helical vortex breakdowns, where they measured negative velocities of the order of 10–25% of the positive velocities. The area averaged velocity expected for the flow rates is around 6 m/s. Thus it is reasonable to assume that the flow field is having negative velocity paths which help the flame travel upstream at these speeds. The expected flame speeds for the preheated turbulent flame can utmost only be of the order of 1–2 m/s. Experimental measurement of this velocity during a precursor event to support the inferences is not easy given the randomness of the events. Computational studies can

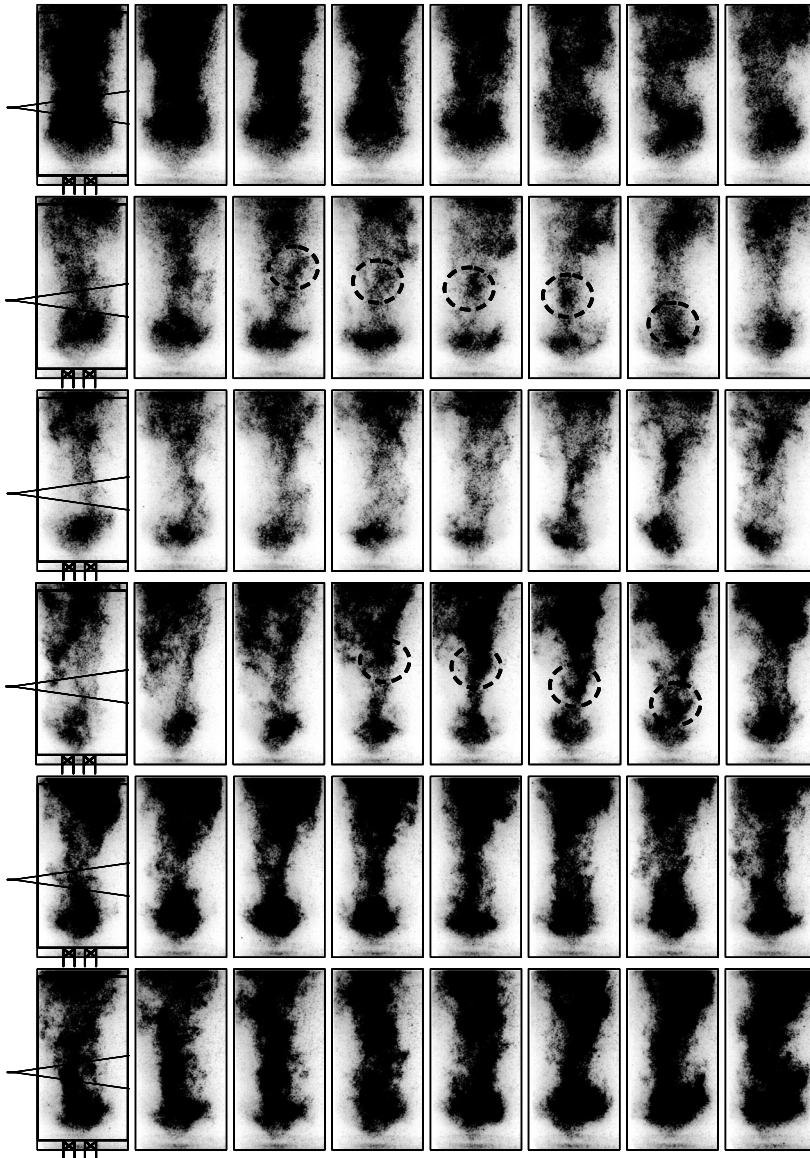


Figure 8: Inverted gray scale movie frames from OH* chemiluminescence emission showing an extinction-reignition event. The images are separated by 0.51 msec. The intensities are multiplied by a factor 1.4 before inversion to enable easy recognition of flame structures. The images in Figure 7(c, 2-7) appear as the left most images in each of the rows, and the image Figure 7(c, 8) follows the last image in this sequence.

throw more light in this direction, if effect of turbulence and flame stretch effects are included.

Figure 9 shows the full sequence of images for the blowout event represented by Figure 7(d). Again, the images were enhanced by multiplying the intensities by a factor to increase contrast. The same multiplying factor has been used for both the precursor event and the blowout event to help comparison. The second image in the sequence Figure 7(d) is the same as Figure 9(a) first row last image. And the last image in Figure 9(c) is the same as the last image in the sequence Figure 7(d).

Compared to the precursor event shown in Figure 8, the IRZ flame is weaker after the extinction phase. Also the double helical structure is not seen until after the middle of the second row in Figure 9(a). The rotating double helical structure of flame is seen near the exit of the combustor, but it does not propagate upstream, until first row of Figure 9(b), while during the whole period, the IRZ flame is becoming more weak and is almost lost by the end of Figure 9(a). When the flame from the rotating double helix reaches the IRZ, the IRZ becomes bright and flame structure recovers in a similar fashion as in the re-ignition phase of the precursor event. This time however, the IRZ does not develop to its full size of a bright blob, and thus the recovered flame is still weak compared to that at the end of a precursor event.

By the end of Figure 9(b), the next extinction phase of the IRZ starts, and the same behavior repeats as before, with the double helical structure even weaker (see Figure 9(c) 2nd row), and the flame propagating towards IRZ is dull. This happens along with the decaying of IRZ, as before, and the lesser preheating of the gases by the colder IRZ may also cause the flame to be weaker. Eventually there is no flame to rejuvenate the IRZ. Even after the flame is lost in the IRZ, the double helical flame structure from the exit of the combustor was seen to try and re-ignite the IRZ a few more times, and subsequently the whole flame is lost by the end of Figure 9(c). The images after this sequence, when enhanced, were showing only the hot walls emitting black body radiation (also seen very lightly in the last two images of Figure 9(c)).

The chemiluminescence imaging can give only the regions of flame and probably a little bit of regions of hot products. When there is no flame in some region of combustor, one cannot ascertain whether that region is filled with reactants or products. In order to understand whether the regions of 'no flame' during these events are filled by cold reactants or hot products, specific experiments were conducted with seeding the premixed mixture with olive oil droplets. The combustor was illuminated with vertical laser sheet to view the distribution of the droplets in the combustor during the precursor events. Oil droplets (size 1–2 microns) evaporate at high temperatures and will not be visible in Mie scattering above around 700 K [43]. If the reactant gas goes through a flame the oil droplets evaporate and the oil probably will also combust. There is very little probability that the evaporated oil can condense back to droplets without active cooling. Thus Mie scattering of these droplets tracks only the cold reactants which have never experienced the hot gases. One must be cautious about the change in equivalence ratio at blowout as the olive oil vapors will also release heat during combustion, along with removing heat from the gases for evaporation. It was found that there was a small decrease (0.02–0.04 lower) in the blowout equivalence

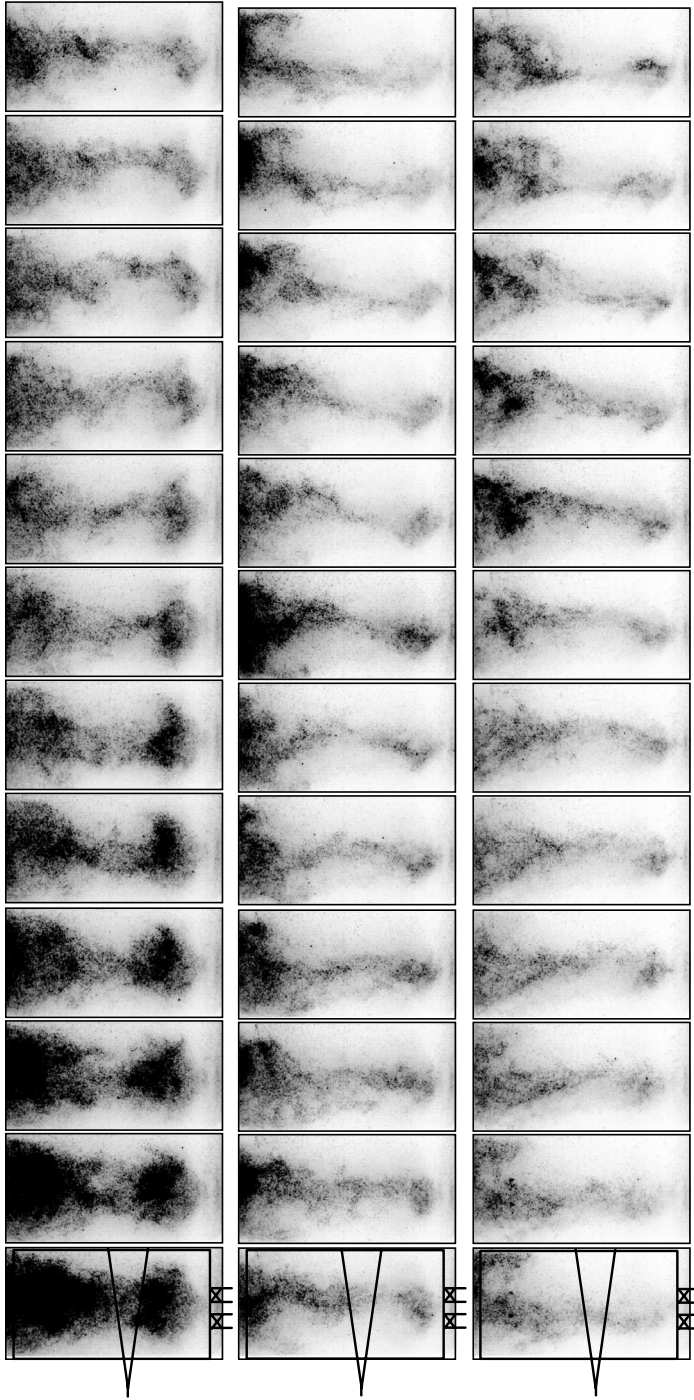


Figure 9(a): Inverted gray scale movie frames from OH^* chemiluminescence emission showing the first part of the full blowout event. The images are separated by 0.51 msec. The intensities are multiplied by a factor 1.4 before inversion to enable easy recognition of flame structures. The images in figure 7(d, 2 & 3) appear as last image in first row, and the third row 4th image in this sequence.

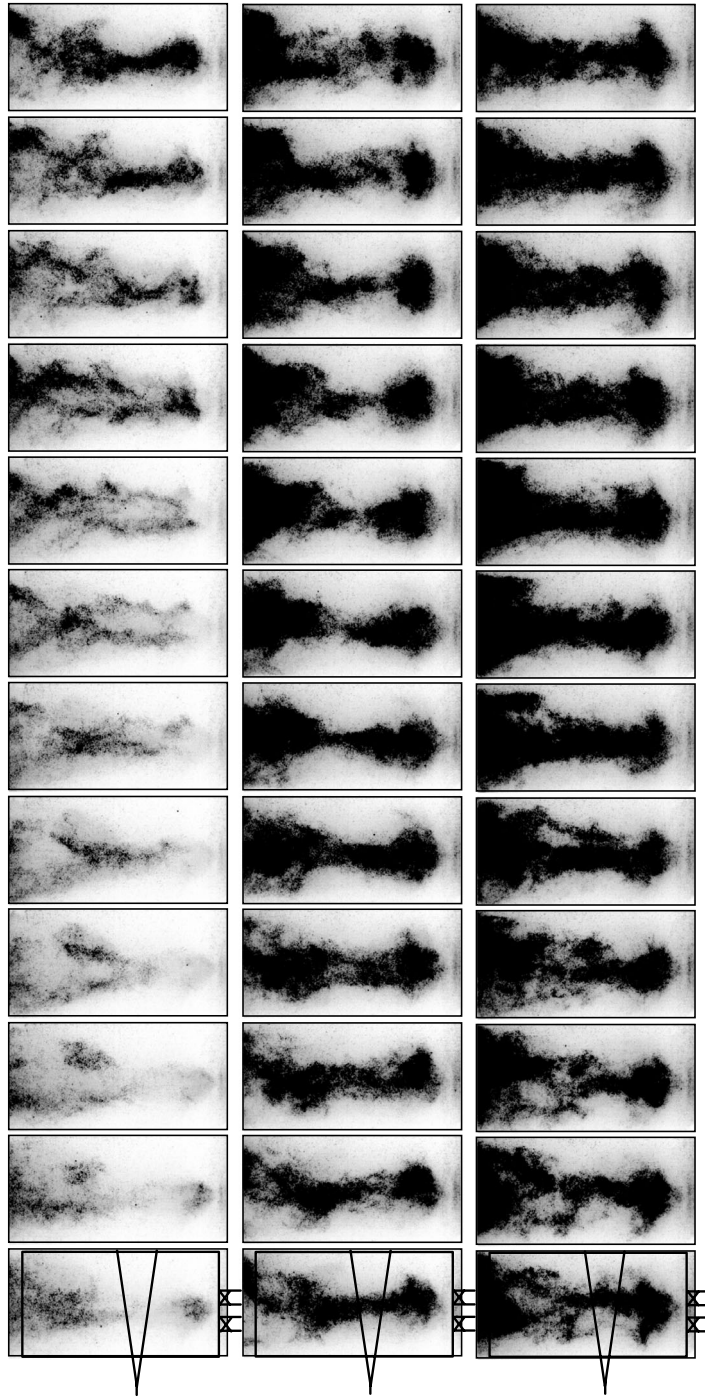


Figure 9(b): Inverted gray scale movie frames from OH^* chemiluminescence emission showing the second part of the full blowout event. These images follow those in Figure 9(a) in the full blowout sequence. The images are separated by 0.51 msec. The intensities are multiplied by a factor 1.4 before inversion to enable easy recognition of flame structures. The images in Figure 7(d, 4 & 5) appear as the eighth image in the first row and the last image in the second row in this sequence.

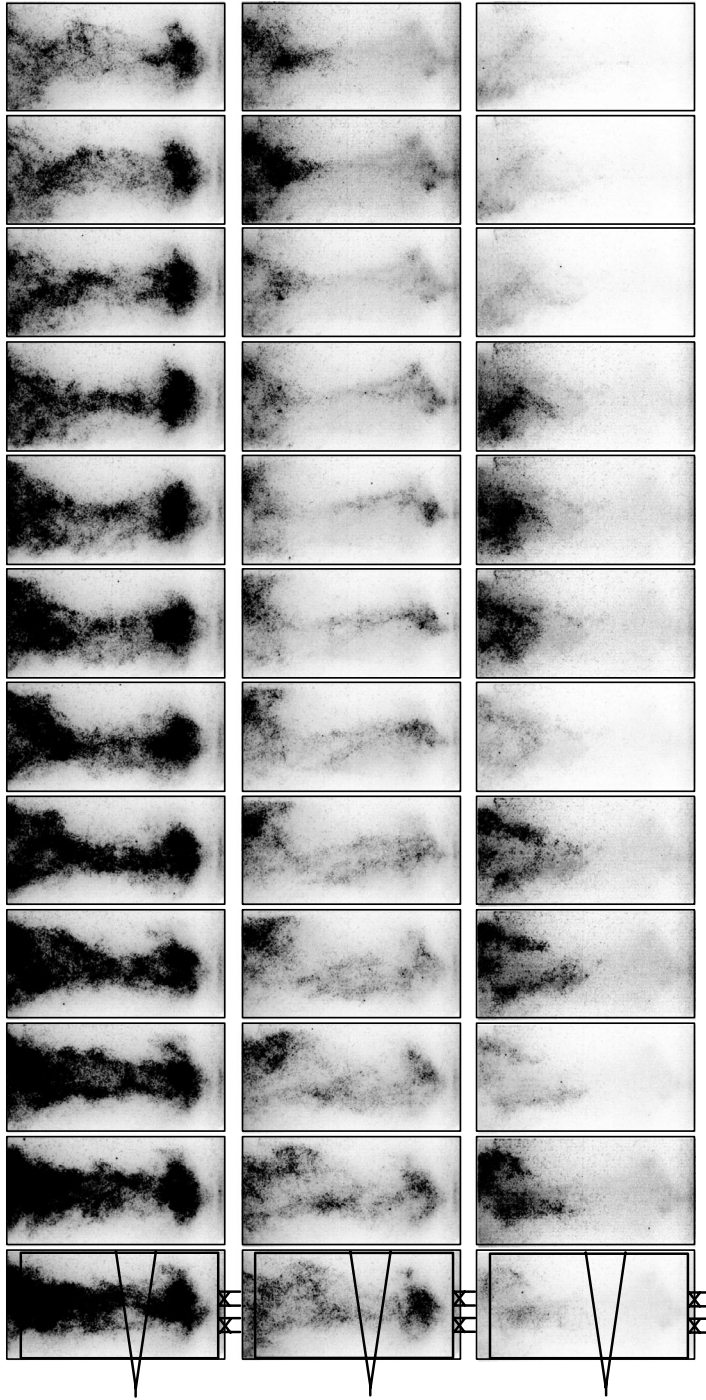


Figure 9(c): Inverted gray scale movie frames from OH* chemiluminescence emission showing the second part of the full blowout event. The images follow those in Figure 9(b) in the full blowout sequence. The images are separated by 0.51 msec. The intensities are multiplied by a factor 1.4 before inversion to enable easy recognition of flame structures. The images in Figure 7(d, 6–8) appear as 4th image in first row, 8th image in second row, and the last image in this sequence.

ratio of the combustor at the flow rates used. The precursor dynamics from OH* chemiluminescence sensor data appeared similar with and without oil droplets. Thus it is reasonable to assume that the combustor dynamics is not affected considerably by seeding the flow with oil droplets. Nevertheless, this technique gives very important information regarding the dynamics of the combustor near blowout.

Figure 10 shows the time series data obtained from the OH* chemiluminescence sensor during the droplet imaging experiment. It can be seen that the signal has a mean of around 0.48, while there are large deviations from it. At around 5 seconds, the flame is lost from the combustor. The bottom row shows the expanded view of the same data during regular combustion, a precursor event, and the blowout event. There were several extinction-reignition events that occurred just prior to the blowout event, as evident from this figure. The flow rates of fuel/air were not changed during the experiment.

Figure 11 shows inverted gray scale images from the high speed droplet Mie scattering movie. Thus the regions of white are hot regions where there are no droplets present and the regions of dark are regions of cold reactants with droplets, darker the colder. All the images have been obtained from a single run with constant conditions, very close to LBO. Since this visualization is with laser sheet passing diagonally

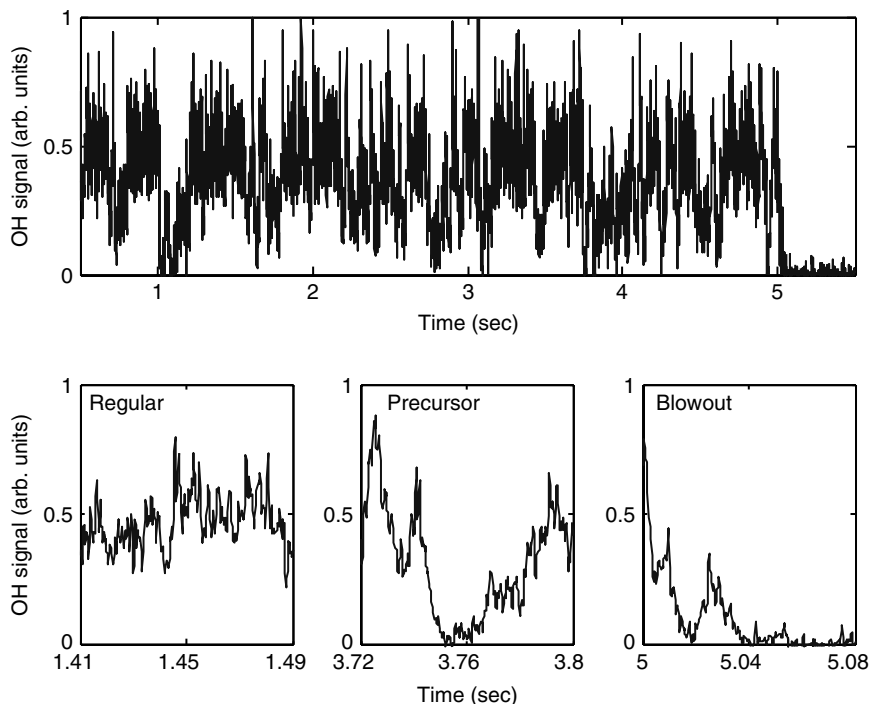


Figure 10: OH* chemiluminescence signal obtained from local chemiluminescence photodiode. The bottom row shows the expanded view of the data.

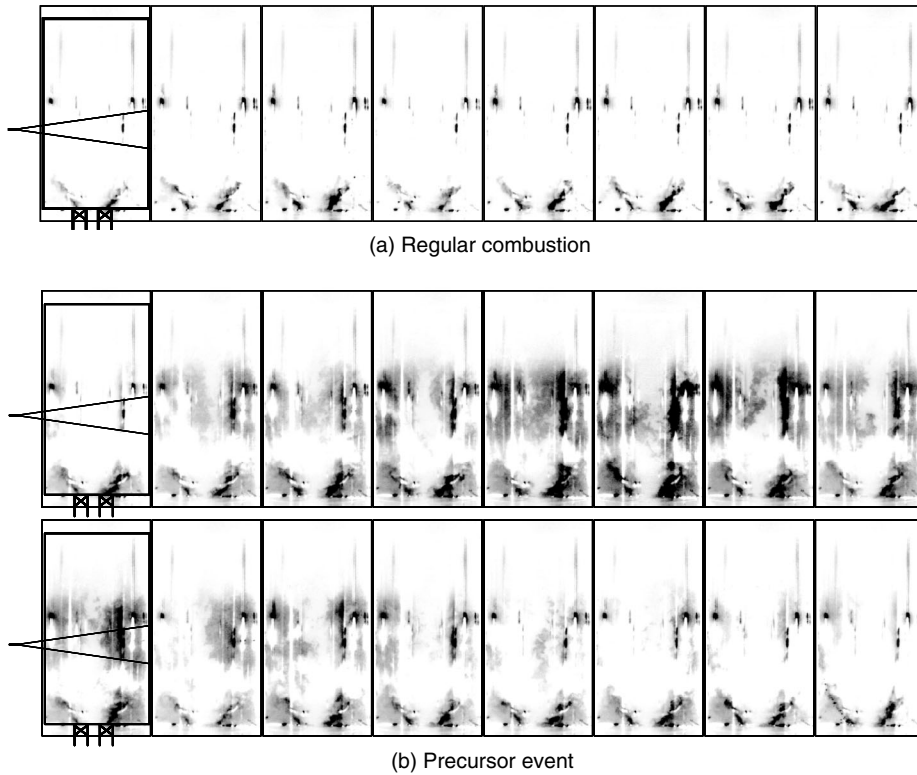


Figure 11: Inverted gray scale movie frames from oil droplet scatter imaging technique showing (a) regular combustion, and (b) a precursor event (two rows). Laser sheet spans only the bottom two-thirds of the combustor height. Regions where droplets are present will be seen as dark, and hot regions are seen as white. The image separation Δt between the images is 2 msec. All these frames are from the same run with constant flow rate and seeding conditions. The vertical lines with dark borders (seen in all the images) are due to laser sheet reflections on circular walls. These cannot be removed by image processing due to saturation of the camera at those pixels. They can be seen very clearly in the last image of Figure 12 where there are droplets filling the combustor after LBO.

through circular tube, there were multiple reflections of the laser (seen as vertical lines) which are seen in all the images. Since the camera saturated in those areas, these lines could not be removed by image processing. Thus the scatter from circular tubes are visible as white vertical lines with dark borders, as seen in the first row images Figure 11 and last two images of Figure 12.

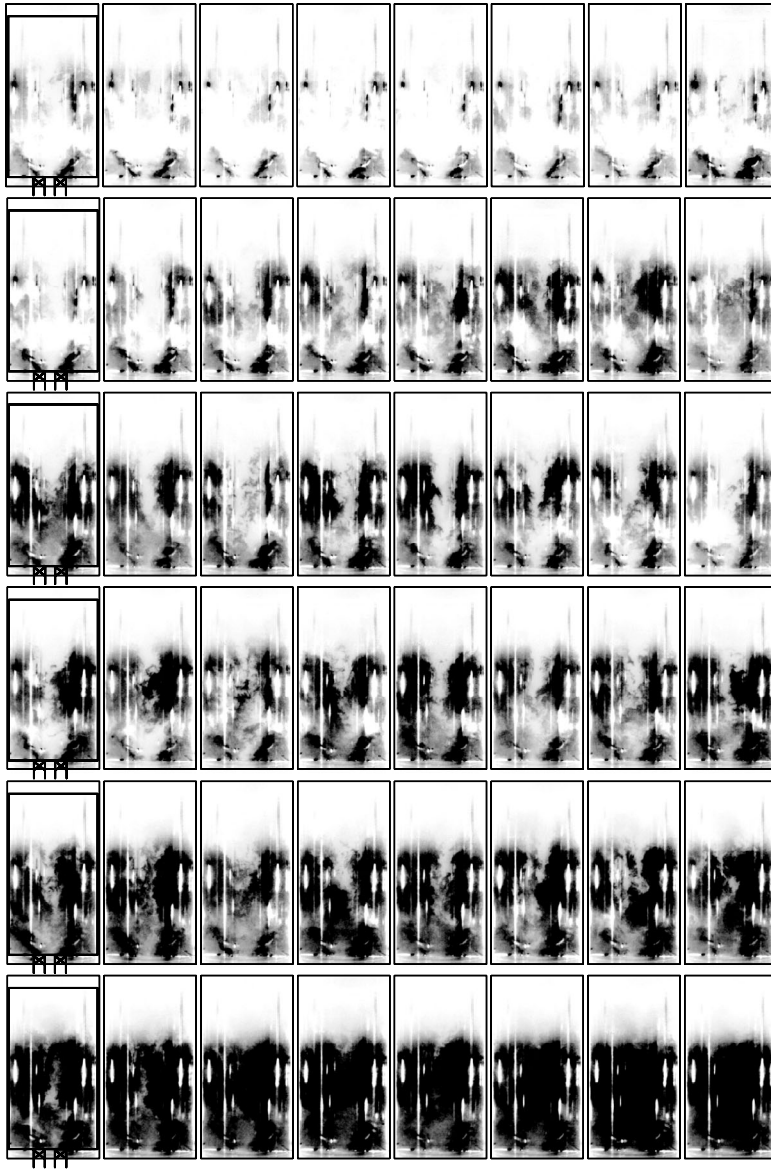


Figure 12: Inverted gray scale movie frames of LBO event from oil droplet scatter imaging technique. Laser sheet spans only the bottom two-thirds of the combustor height. Regions where droplets are present will be seen as dark, and hot regions are seen as white. All these frames are from the same run as that in Figure 11. The image separation Δt between images is 1 msec.

Images in Figure 11(a) show a sequence of regular combustion. It can be seen that there are droplets coming out of the annular inlet in a conical shape with both inner and outer shear layers visible in the edges of the droplet stream. This reveals that the combustor is filled with hot gases in both IRZ and ORZ even when there is no flame visible in the ORZ (when close to LBO). When we move closer to LBO, the ORZ starts getting some droplets, showing light gray, suggesting that the ORZ is getting colder. Figure 11(b) shows the sequence of images with a precursor event for the same conditions. It can be seen that the droplets start filling the ORZ and then move around the IRZ and fill the region above IRZ. IRZ though decreasing in size is still hot and without any droplets, while the region above has cooled down. This observation along with that from our previous observation in Figure 8 shows that the flame is lost in that region and the region is occupied by cold reactants. At the end of the extinction phase of the precursor event, the IRZ also is cooling down as indicated in Figure 11(b-5, 6) by the weak gray in IRZ.

After this partial extinction phase of the precursor event, one can observe streaks of hot gases appearing above the IRZ. One should keep in mind that we are visualizing the droplets in a diagonal plane and rotating helical patterns will appear as slant lines translating and oscillating in space, in the cross section. From these images, one cannot judge the motion of the gas packets. Nevertheless, one can observe that there are two slant streaks of hot gases above the IRZ in the 7th image in the precursor event sequence. Following the hot streaks reaching the IRZ, the IRZ gets hotter and expands to occupy larger volume, and then restore the regular combustion. These images were correlated with the OH* chemiluminescence signals to ensure that we are looking at precursor events. This was needed since the narrow band pass filter used in droplet imaging allows only the light of laser wavelength to enter the camera, and thus there is no direct flame visible. The above described phenomenon was observed in all the precursor events and there were more of them as the LBO is approached. The partial precursor events shown in chemiluminescence images cannot be detected clearly from the droplet images due to low intensity levels from (presumably) regions of colder gases. This may be due to the fact that the IRZ is still very strong in flame intensity and size (as shown in Figure 7(b)), and the droplets don't survive while the reactants go around the IRZ.

Figure 12 shows the sequence of images during a full blowout event. The process of extinction starts similar to the extinction phase of a precursor as described in Figure 11(b). The droplets surround the IRZ and the IRZ diminishes in size. The second row in Figure 12 shows that the IRZ becomes weaker than that in a precursor event, allowing more droplets to survive the temperature. The third row shows the streak of hot gases extending from the top towards the IRZ. (One should keep in mind that this is planar cross section imaging) By the end of third row, the IRZ becomes strong, but could not stay strong for long. The hot packets coming downwards this time is surrounded by colder reactants and the flame becomes weaker by the time it reaches IRZ. As a result, IRZ does not recover, and is getting colder. This observation is a parallel to support the observation from chemiluminescence blowout sequence shown earlier. This whole process of flame packets approaching IRZ from exit happens a few times with progressively weaker and weaker flame packets and IRZ eventually loses its hot gases. IRZ finally becomes dark and the flame is lost from inside the combustor after that. The weak double helical flame structure in last row of Figure 9(c) is not seen here because of the limited height of the laser sheet.

It can be noted that the walls are still hot and the droplet intensities are lesser near the walls and in ORZ. The behavior described above is very repeatable near LBO at different flow rate conditions in the combustor. There are a few droplet scatter images which can also support the double helical structure observed in chemiluminescence imaging. In Figure 12, image 7 of 2nd row, image 6 of 3rd row, images 3 & 8 of 4th row, and images 7 & 8 of 5th row show possible evidence of double helical flame structure.

To understand the behavior further, horizontal cross section of droplet distribution was obtained using horizontal laser sheet, at different heights from the inlet. The results presented here are from only one height of 1" from the inlet (see Figure 3). The camera was viewing through a mirror from above the combustor exit and was recording at 3000 frames/sec. These droplet visualization images were not inverted as the intensities near blowout are better with the direct image. Thus in these images, bright corresponds to presence of droplets, which corresponds to cold reactants present in that location. Figure 13 shows three sequences corresponding to regular combustion, a precursor event and blowout event. These events were again identified by simultaneous OH* sensor data from the fiber probe. The last image in the whole sequence shows the combustor filled with cold flow and also shows the edge of the combustor in each image. The dark circular region around the combustor was superimposed in all the images to help the reader visualize the flow field boundaries.

Figure 13(a) shows the sequence during regular combustion, showing that most of the combustor is devoid of droplets, suggesting the combustor is filled with hot gases in that plane. Figure 13(b) shows an extinction-reignition event. The droplets surround the IRZ which is still hot, forming an annular colder region in the combustor. This matches with the observation that the droplets go around the IRZ prior to the extinction phase. During the extinction phase, the droplets slowly fill the central hot region and the IRZ diminishes in size. The IRZ is almost completely cold in image 8 in this sequence. Two milliseconds after this, there appear two hot zones in the droplets, which expand and become one big hot zone. The IRZ again gets weaker a little but is restored subsequently to regular combustion. There were a few images in the sequence omitted before this sequence shown, which shows the growth of the annular region around the IRZ slowly from regular combustion situation.

Figure 13(c) shows the blowout event as visualized by horizontal cut droplet scattering method. The first row shows the extinction phase which is similar to the extinction phase of the precursor event. In this case, the two hot zones don't appear immediately. Image 7 in the first row shows a sign of two hot zones, with one of them weaker. Even the stronger one subsequently dwindles. The zones are seen to rotate anticlockwise, due to the swirl of the overall flow. In the second row, it can be seen that the hot zone is completely lost and a single hot zone appears to have returned, followed by another hot zone appearing to its side in image 9. These hot zones are surrounded by droplets that are brighter than those surrounding the hot zones in reignition sequence of a precursor event. This suggests that the droplet region is colder in blowout sequence than in precursor sequence. These hot zones are soon quenched by the cold gases around, and again there exists only cold gases at that section, as seen in the beginning of the third row. There appears another hot zone which is even weaker than before, which is also quenched and the combustor loses flame after this. The images following this sequence are all filled with droplets fully and the

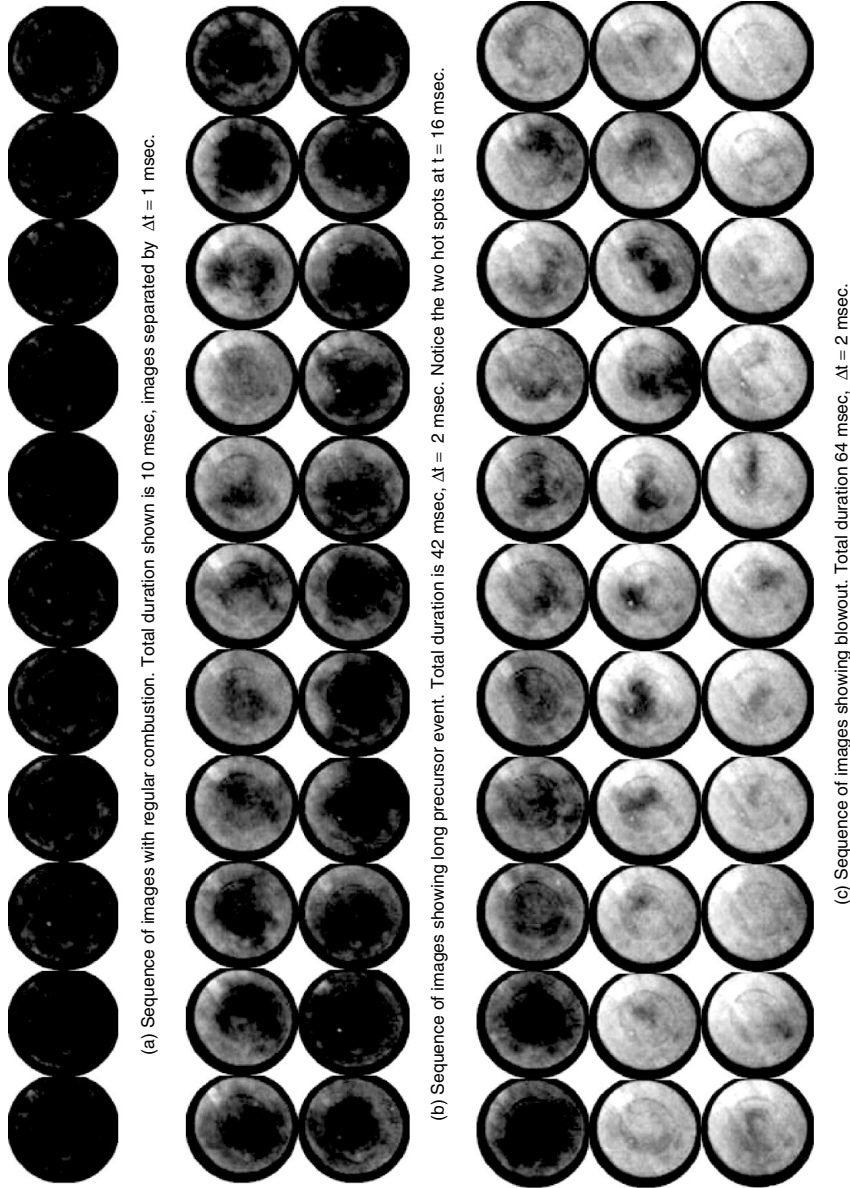


Figure 13: Sequence of horizontal plane droplet visualization movie frames for (a) regular combustion, (b) long precursor and (c) blowout. The dark circular region around the combustor was superimposed in all the images to help the reader visualize the flow field boundaries.

intensity of the image becomes more and more bright. This is due to cooling down of the combustor and the droplets staying at larger size and scattering more light.

Figure 14 shows the complete image sequence during the reignition phase shown in Figure 13(b). The sequence starts one millisecond after image 8 in Figure 13(b). Images 4 & 10 in this sequence are same as images 9 & 10 in Figure 13(b). This sequence shows the growth of two hot zones clearly. One of them appears to be hotter than the other. Both are growing in size to merge and become one big hot zone, in image 7. Soon this hot zone shape changes to more circular one in image 10. This along with vertical sheet images and the chemiluminescence images, show that two separate hot regions propagate upstream along helical paths and restore the IRZ. When the IRZ is hot enough, it expands and occupies the original volume and restores the ‘V-shaped’ flame. And when this restoring flame is not strong enough, it is quenched before it could restore the IRZ and thus the flame is lost in the combustor. There were several runs of this horizontal sheet experiment where the two hot zones were observed, and occasionally, the two hot zones appeared one after the other, but leading to the same final outcome. This suggests that the flame propagation along the two rotating helical structures need not be equal in strength.

Since the flame mode would transition to a ‘tornado’ mode if the combustor were longer and the flame shape (visual observation) during the long precursor events appeared similar to the tornado flame, a tornado flame in longer combustor was studied using high speed camera. Figure 15 shows frames that cover the full length of the longer quartz tube (8”) combustor. The airflow rate used was the same, but the equivalence ratio was lower than the blowout limit of the 5” combustor. The movie was recorded at 1.9 kHz and 100 μ sec gate time. The frames shown here are separated by roughly 1.1 milliseconds. The last image shown is an average image averaged over 105 msec, including frames 1–7. The images show a stable region of combustion at downstream end of the combustor. The two vertical lines seen in all the images at about 1/4th width from either side are reflections of stray light by circular quartz walls of the combustor.

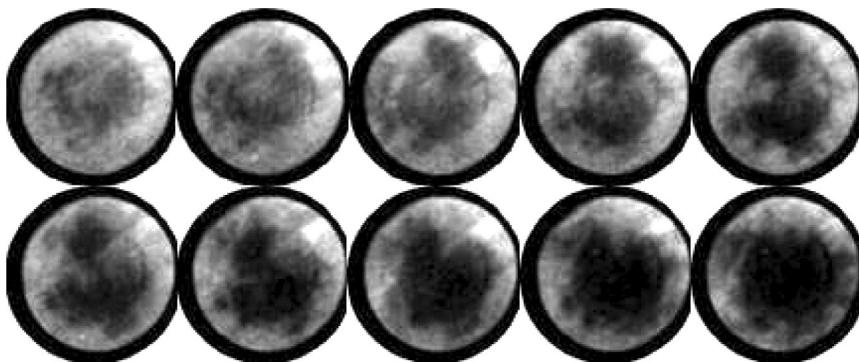


Figure 14: Sequence of horizontal plane movie frames showing the reignition phase of a precursor event. Total duration 3 msec, $\Delta t = 0.33$ msec. Notice the two hot spots swirling, growing and merging in the images.

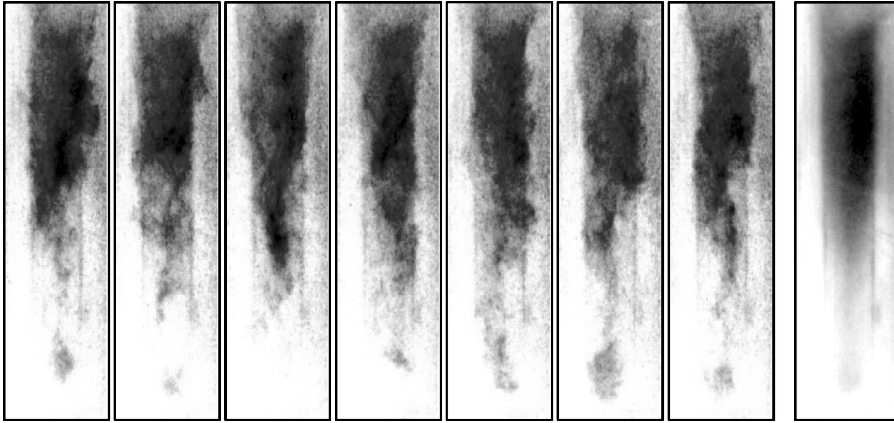


Figure 15: Sequence of (inverted grayscale) chemiluminescence images near inlet of longer combustor with equivalence ratio 0.75 (below LBO limit of short combustor). The images are separated by 1.1 msec. The last image is an average of frames over 105 msec. The vertical lines are due to reflection of the stray light from circular tube.

Bradley *et al.* [44] have shown that this mode of combustion is mainly stabilized by the hot walls of the combustor. The images show that there appears to be a double helix shaped flame rotating due to the swirl. The rotating double helix structure can be recognized in frames 3–5. Frames 3 & 4 show side view of the two helical structures rotating about each other. Frames 4–6 show a small packet of the flame being convected towards the inlet of the combustor. These double helical shapes are similar to those observed in the reignition phase of the precursor event in the 5" combustor. However, the double helical flame structure was observed clearly before, only during the precursor events. These observations suggest that the recovery mechanism used by the flame during the precursor event, is through this tornado flame mode (which is stabilized in the shorter combustor, at least temporarily, by the hot walls). The speed of propagation of these packets downward calculated earlier suggests that flame takes certain negative velocity helical paths in the flow field during the reignition phase of the precursor event. Similar flame movement was also observed by Ishizuka [45].

Figure 16 shows an illustration of the dominant mode of the velocity field in the double helical VBD [38]. The flow field can be visualized as two pairs helical flow tubes with flow direction alternating upwards and downwards (see Figure 16(a)). This flow structure rotates in time, about the axis of the combustor, due to swirl. The hot gases which were convected downstream during regular combustion, now convect upstream through the negative velocity flow tubes. This can cause mixing of hot products and colder reactant gases at the shear layer between these flow tubes and cause a flame. This flame would propagate into the unburned gases from the interface between the hot and cold flows. This is illustrated in Figure 16(b). This downward propagation of the flame into the upward flow causes a stationary structure of the flame that appears to be a fixed

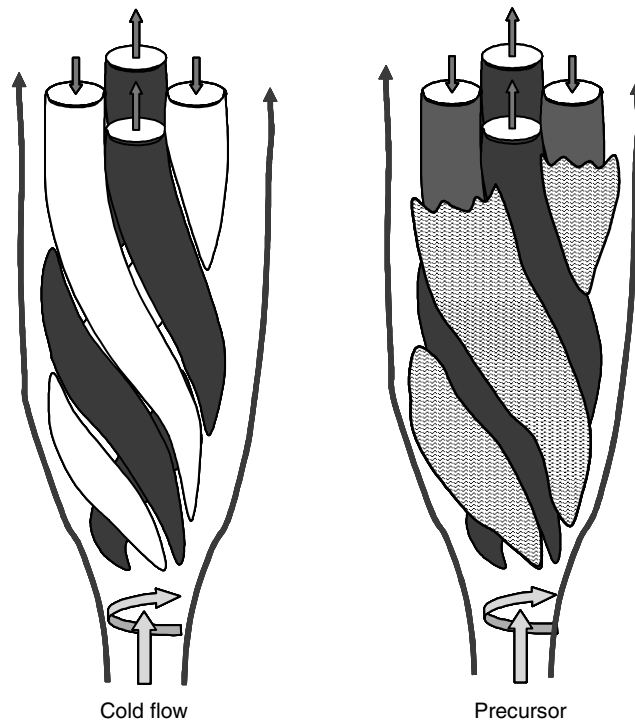


Figure 16: Illustration of flow field in the helical flame mode. (a) Cold flow field showing alternating upward and downward flow tubes (b) Hot flow field showing the cold reactants in darker flow tubes and hot products in reverse flow direction in lighter flow tubes. The flame propagates into the reactant tubes from the interface between the hot and cold flow tubes.

helical path just rotating about the axis (due to rotation of the helical structure). Disturbances in the flow field can cause lower velocities in the unburned flow which permit flame packets to reach the inlet occasionally. This flame holding mechanism was also explained further by Ishizuka [45] in his review of different theories of flame propagation in vortex core against flow direction. This explains the behavior of the tornado flame, and along with the previous observations in precursor events, also justifies that helical VBD occurs following the extinction phase of a precursor or a blowout event.

The only piece of the puzzle to be explained is the mechanism for the changes in the VBD mode. One should recall from section 2, that the switch from bubble to helical mode occurs when the transfer of axial momentum to the radial direction decreases, and helical to bubble VBD when the transfer increases [40]. The proposed mechanism is that the flame becomes weaker locally and there are local extinctions in the flame around the IRZ. This causes the cold reactants to go through the flame envelop and surround the

IRZ. This causes the IRZ to cool down and thus the flame becomes further weaker unless the disturbances are short lived.

When the heat release in the IRZ decreases, the convective forces overcome the dilatation and decrease the size of the IRZ. The streamlines need not diverge as much as when there was more dilatation (heat release). This decreases the radial component of velocity, which in turn impedes the transfer of axial vorticity into circumferential vorticity that is required for bubble type VBD. Thus the bubble loses “strength” and shrinks in size. This further increases the axial component of velocity at inlet and thus forms a bootstrapping mechanism that leads to forming the helical VBD.

The mechanism for the transition from the spiral VBD mode back to the bubble mode would be quite the opposite. When the hot gases return to a region near the inlet through the tornado flame mode, the dilatation from the heat release would cause the incoming streamlines to diverge. This would increase the radial velocity near the inlet and assist in redistribution of axial vorticity into circumferential vorticity. This would further decrease the axial velocity component and thus induce the streamlines to diverge more. The recirculation of the hot gases thus caused, also helps increase the strength of the combustion process and increases the dilatation. Overall, this process has positive feedback and would lead to recovery of the bubble type VBD. In case the recirculation thus caused does not have enough hot gases to entrain, the system may not become stronger, and eventually revert back to the helical VBD mode.

5. FULL SEQUENCE OF BLOW OUT EVENT

The observations presented in previous sections can be put together to form a complete sequence of the flame dynamics near blowout of a swirl-dump stabilized combustor. This section summarizes the overall blowout process of the combustor including findings from previous works by the authors of this work and others.

The V-flame is stabilized by the bubble type vortex breakdown, which forms the IRZ. The incoming premixed gases go around the IRZ and start mixing, in a turbulent manner, with the gases from inside the IRZ. (See Figure 17(a)) Some hot packets that leave the IRZ enter the reactant gas stream and ignite the gases. These gases now follow the streamlines around the IRZ and burn. Some of these new product gases enter the IRZ from its downstream end. Thus the IRZ has a continuous inflow and outflow of radicals and heat. The remaining reactant gases and products go past the IRZ and are convected out of the combustor. These gases will flow along the walls of the combustor as they burn, keeping the walls hot.

When the mixture is made leaner, the heat release decreases and thus the sustaining exchange of fresh radicals and heat is decreased. The flame is weaker and takes longer to completely burn the reactants, by which time the gas packets have been convected past the top of IRZ. This will cause exchange of partially burnt mixture into the IRZ. Small intermittent perturbations, possibly due to local extinctions of the flame (near the inlet side of IRZ) due to high strains, may also cause the entrainment into the IRZ to consist of colder gases or less effective ignition sources. (see Figure 17(b)) Thus the IRZ becomes colder and less able to ignite the surrounding reactants. Thus there may be packets of reactants just convected around the IRZ and through the exit of the combustor.

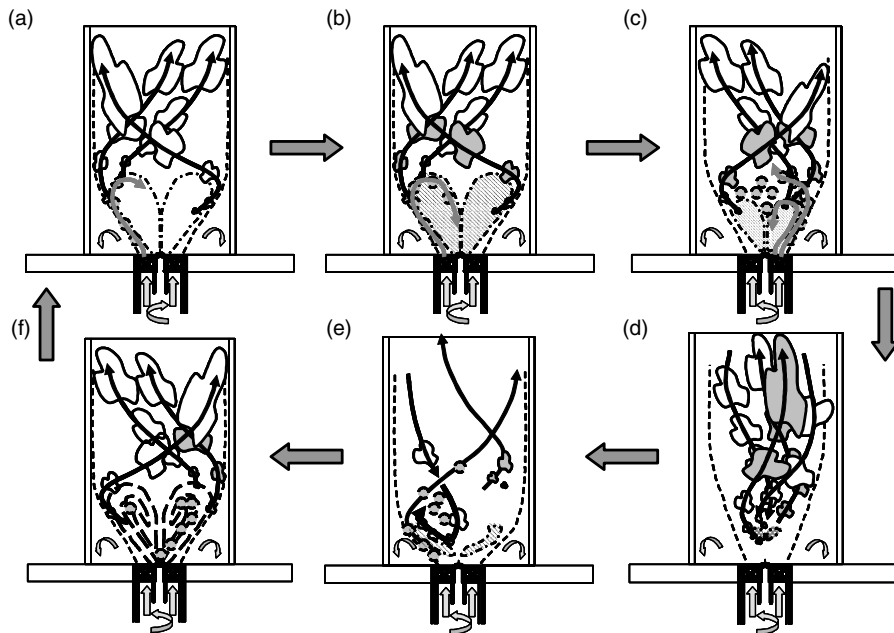


Figure 17: Sketch illustrating the mechanism of blowout dynamics in the swirl dump combustor. The top left corresponds to regular combustion. Darker spots represent colder reactant packets.

This causes more cold packets to enter the IRZ and weaken it further. There comes a point in time when there are enough cold packets entering (and leaving) the IRZ that the reactants outside are occasionally not ignited. This forms a hole in the stream of burning gases convected downstream of the IRZ. (See Figure 17(c)) This causes the partial precursor events described earlier, if the flame returns back to system shown in Figure 17(a) → (b) subsequently. The region of unburnt gases at the top of the IRZ also causes cold reactant packets to enter the IRZ from the top.

The probability of local extinctions increases as the equivalence ratio is decreased and the overall flow rate is maintained. This causes the number of times the partial precursors occur, to increase, causing the IRZ to cool down more and thus most of the packets that leave the IRZ are now ineffective in igniting the outer mixtures. IRZ is now enveloped by cold gases and the IRZ gets colder. The decreased dilatation causes the bubble type VBD to decrease in size. This causes more packets around the IRZ to be convected without ignition, causing large regions of no combustion. This is the extinction phase of the precursor/blowout event.

When the extinction phase is nearly complete, the bubble decreases in size which decreases the redistribution of axial momentum into radial direction. The onset of bubble-to-helical type VBD mode shift occurs. (See Figure 17(d)) This creates a path for hot gases from further downstream to return through the helical negative velocity

paths. These packets could start a reaction near the inlet and cause heat release (and thus expansion) to occur. This dilatation (see Figure 17(e)) starts the positive feedback for the formation of bubble type VBD mode. This causes the IRZ to develop again, thus restoring the regular flame shape. (See Figure 17(f)) This is the reignition phase of the precursor event.

The formation of bubble type VBD mode depends mainly on starting a heat release reaction near the inlet. This depends on the equivalence ratio and temperature of the incoming mixture, and the heat content and radical concentration in the burnt gas packets moving upstream through the negative velocity paths. The burning packets of gas that was convected downstream during regular combustion just prior to the extinction phase may lose heat to the walls and may not be effective in igniting the mixture when convected upstream through the negative velocity paths. The walls, which were maintained at a high temperature during regular combustion, are cooling down since there are non-burning packets flowing near them. Thus after a few consecutive occurrences of these precursor events, the walls may become cold enough to cause enough heat losses that the hot gases propagating upstream has a higher chance of not causing sufficient heat release and does not effect the transition to bubble type VBD.

It may also be due to a large delay in the formation of the negative helical paths during which time, the hot gas packets that were at the end of the combustor are now replaced by colder reactants which are just convected to the end of the combustor, and thus the returning packets are colder. Thus the reignition process is not completed and thus the flame never recovers, causing blowout. In a longer combustor, the double helical VBD mode gets preheated gases due to hot walls which can now burn and thus could sustain the tornado mode of the flame, a little longer.

6. CONCLUSIONS

This paper presented a set of results from various experiments in a swirl-dump stabilized combustor operating at atmospheric conditions, near its LBO limit. The chemiluminescence movie images were used to understand the movement of the flame zones, while the oil droplet imaging was used to understand the non-burning zones. This along with results from other works in combustion-VBD interaction, a full mechanism for the dynamics of the flame near blowout of the combustor was presented. The mechanism is consistent with the behavior of the swirl dump stabilized combustor near blowout, as observed from previous works. It was shown that the phenomenon was due to the coupling of combustion process with the vortex breakdown mode switching processes. Flame is primarily stabilized by recirculation associated with a bubble-type vortex breakdown in 'V-flame' and double helical mode in the 'tornado flame'.

This process explained above is the mechanism used by the flame near the critical conditions where fluctuations in the system can create oscillations between the two possible solutions (a bifurcation). These oscillations near the bifurcation of the flame structure, were observed as precursor events or lower order chaotic behaviors, and were used to estimate the proximity to blowout, in earlier works. When the system is closer

to critical point, even small disturbances can cause switching between possible solutions, and thus more events can be expected when closer to the blowout event. This theory is consistent with the behavior of the combustor near blowout as observed in previous sensing and control experiments. This paper is the first detailed experimental study of the unsteady dynamics that occur near blowout of a swirl dump stabilized combustor.

REFERENCES

- [1] Richards, G. A., McMillian, M. M., Gemmen, R. S., Rogers, W. A., and Cully, S. R., "Issues for Low-Emission, Fuel-Flexible Power Systems", *Progress in Energy and Combustion Science*, Vol. 27, 2001, pp. 141–169.
- [2] Lefebvre, A. H., "Gas Turbine Combustion", Edwards Brothers, Ann Arbor, MI, 1999.
- [3] Law, C. K., "dynamics of stretched laminar flames", *Proc. Comb. Inst.*, Vol. 22, 1988, pp. 1381–1402.
- [4] Ghoniem, A. F., Soteriou, M. C., Knio O. M., and Cetegen, B., "Effect of steady and periodic strain on unsteady flamelet combustion", *Proc. Comb. Inst.*, Vol. 24, 1992, pp. 223–230.
- [5] Im, H. G., Bechtold, J.K., and Law, C. K., "Response of counterflow premixed flames to oscillating strain rates", *Combustion and Flame*, Vol. 105, 1996, pp. 358–372.
- [6] Sardi, K., Taylor, A. M. K. P., and Whitelaw, J. H., "Extinction of turbulent counterflow flames under periodic strain", *Combustion and Flame*, Vol. 120, 2000, pp. 265–284.
- [7] Sardi, K. and Whitelaw, J. H., "Extinction timescales of periodically strained lean counterflow flames", *Experiments in fluids*, Vol. 27, 1999, pp. 199–209.
- [8] Nicholson, H., and Field, J., "Some Experimental Techniques for the Investigation of Mechanism of Flame Stabilization in the Wakes of Bluff bodies", *Proceedings of the Combustion Institute*, The Combustion Institute, Pittsburg, PA, Vol. 3, 1951, pp. 44–68.
- [9] Chao, Y. C., Chang, Y. L., Wu, C. Y., and Cheng, T. S., "An Experimental Investigation of the Blowout Process of a Jet Flame", *Proceedings of the Combustion Institute*, The Combustion Institute, Pittsburg, PA, Vol. 28, 2000, pp. 335–342.
- [10] Hedman, P. O., Fletcher, T. H., Graham, S. G., Timothy, G. W., Flores, D. V., and Haslam, J. K., "Observations of Flame Behavior in a Laboratory-Scale Pre-mixed Natural Gas/Air Gas Turbine Combustor from PLIF measurements of OH", Paper No. GT-2002-30052, *Proceedings of ASME TURBO EXPO 2002*, Jun 3–6, Amsterdam, Netherlands, 2002.
- [11] Chen, T. H., Goss, L. P., Talley, D., Mikolaitis, D., "Stabilization zone structure in jet diffusion flames from liftoff to blowout", paper AIAA-89-0153, *27th Aerospace Sciences Meeting*, Reno, NV, Jan 9–12, 1989.

- [12] Shih, W.-P., Lee, J. G., and Santavicca D. A., "Stability and emissions characteristics of a lean premixed gas turbine combustor", *Proceedings of the Combustion Institute*, The Combustion Institute, Pittsburg, PA, Vol. 26, 1996, pp. 2771–2778.
- [13] Roquemore, W. M., Reddy, V. K., Hedman, P. O., Post, M. E., Chen, T. H., Goss, L. P. Trump, D., Vilimpoc, V., and Sturgess, G. J., "Experimental and theoretical studies in a gas-fueled research combustor", paper AIAA-91-0639, *29th Aerospace Sciences Meeting*, Reno, NV, Jan 7–10, 1991.
- [14] Korusoy, E., and Whitelaw, J. H., "Effects of wall temperature and fuel on flammability, stability, and control of ducted premixed flames", *Comb. Sci. Technol.*, Vol. 176, 2004, pp. 1217–1241.
- [15] De Zilwa, S. R. N., Uhm, J. H., and Whitelaw, J. H., "Combustion oscillations close to the lean flammability limit", *Comb. Sci. Technol.*, Vol. 160, 2000, pp. 231–258.
- [16] Gutmark, E., Parr, T. P., Hanson-Parr, D. M., and Schadow, K. C., "Simultaneous OH and Schlieren visualization of premixed flames at the lean blow-out limit", *Experiments in fluids*, Vol. 12, 1991, pp. 10–16.
- [17] Bayliss, A., Leaf, G. K., and Matkowsky, B. J., "Pulsating and chaotic dynamics near the extinction limit", *Comb. Sci. Technol.*, Vol. 84, 1992, pp. 253–278.
- [18] Gorman, M., El-Hamdi, M., and Robbins, K. A., "Chaotic dynamics near the extinction limit of a premixed flame on a porous plug burner", *Comb. Sci. Technol.*, Vol. 98, 1994, pp. 47–56.
- [19] A. Uppal and W. H. Ray, "On the dynamic behavior of continuous stirred tank reactors", *Chemical Engineering Science*, Vol. 29, 1974, pp. 967–985.
- [20] A. Di Benedetto, F. S. Marra, G. Russo, "Bifurcation analysis of lean premixed combustion of hydrogen/propane mixtures", *Combustion Science and Technology*, Vol. 177, No. 2, 2005, pp. 413–434.
- [21] Yi, T., Gutmark, E., Walker, B., "Stability and Control of Lean Blowout in Chemical Kinetics-Controlled Combustion Systems", *Combustion Science and Technology*, Vol. 181, No.2, 2009, pp. 226–244.
- [22] Muruganandam, T. M., Nair, S., Neumeier, Y., Lieuwen, T. C., Seitzman, J. M., "Optical And Acoustic Sensing Of Lean Blowout Precursors", AIAA 2002–3732, *38th AIAA Joint Propulsion Conference*, 2002.
- [23] T. M. Muruganandam and J. M. Seitzman, "Optical sensing of Lean blowout precursors in a premixed swirl stabilized dump combustor", paper no. GT 2003-38104, *Proceedings of AMSE/IGTI Turbo Expo 2003*, Jun 16–19, 2003 Atlanta GA
- [24] M. Thiruchengode, S. Nair, S. Prakash, D. Scarborough, Y. Neumeier, T. Lieuwen, J. Jagoda, J. Seitzman, and B. Zinn, "An Active Control System for LBO Margin Reduction in Turbine Engines", AIAA 2003-1008, *41st AIAA Aerospace sciences meeting and exhibit*, 2003.
- [25] Muruganandam, T. M., Nair, S., Scarborough, D., Neumeier Y., Jagoda, J., Lieuwen, T., Seitzman, J., and Zinn B.T., "Active control of lean blowout for

- turbine engine combustors”, *Journal of Propulsion and power*, Vol. 21, No.5, 2005, pp. 807–814.
- [26] T. M. Muruganandam and J. M. Seitzman, “Origin of lean blowout precursors in swirled gas turbine combustors”, paper AIAA 2005-1163, 43rd AIAA Aerospace Sciences Meeting & Exhibit, Reno, Nevada, 10–13 January, 2005.
- [27] Lilley, D. G., “Swirl flows in combustion: a Review”, *AIAA JI.*, Vol. 15, No. 8, 1977, pp. 1063–1078.
- [28] Baker, R. J., Hutchinson, P., Khalil, E. E., and Whitelaw, J. H., “Measurements of three velocity components in a model furnace with and without combustion”, *Proc. Comb. Inst.*, Vol. 15, 1975, pp. 553– 559.
- [29] Chigier, N. A., and Dvorak, K., “Laser anemometer measurements in flames with swirl”, *Proc. Comb. Inst.*, Vol. 15, 1975, pp. 573–585.
- [30] J. J. Choi, Z. Rusak and Ashwani K., “Numerical Simulations of Premixed Combustion with Swirl”, paper no. AIAA 2004-977, 42nd AIAA Aerospace Sciences Meeting and Exhibit, Jan 5–8, 2004, Reno, Nevada, USA.
- [31] Z. Rusak, A. K. Kapila and J. J. Choi, “Effect of combustion on near-critical swirling flow”, *Combustion Theory and Modeling*, Vol. 6, 2002, pp. 625–645.
- [32] Y. Huang and V. Yang, “Bifurcation of flame structure in a lean-premixed swirl-stabilized combustor: transition from stable to unstable flame”, *Combustion and Flame*, Vol. 136, 2004, pp. 383–389.
- [33] C.O. Paschereit, P. Flohr, E. J. Gutmark, “Combustion control by vortex breakdown stabilisation”, *ASME transactions: Journal of Turbomachinery*, 2006, Vol. 128, pp. 679–688.
- [34] Lucca-Negro O., and O’Doherty T., “Vortex breakdown: a review”, *Prog. Energy and Comb. Sci.*, Vol. 27, 2001, pp. 431–481.
- [35] Sarpkaya T., “On stationary and traveling vortex breakdown”, *Jl. Fluid Mech.*, Vol. 45, 1971, pp. 545–559.
- [36] Faler J. H., and Leibovich S., “Disrupted states of vortex flow and vortex breakdown”, *Phys. Fluids*, Vol. 20, 1977, pp. 1385–1400.
- [37] Escudier M.P., “Vortex breakdown: observations and explanations”, *Prog. Aerospace Sci.*, Vol. 25, 1988, pp. 189–229.
- [38] Ruith M. R., Chen P., Meiburg E., and Maxworthy T., “Three-dimensional vortex breakdown in swirling jets and wakes: direct numerical simulation”, *Jl. Fluid Mech.*, Vol. 486, 2003, pp. 331–378.
- [39] Althaus W., and Weimer M., “Review of the Aachen work on vortex breakdown”, in dynamics of slender vortices, Krause E., and Gersten K. (Eds.), IUTAM symposium on dynamics of slender vortices, Kluwer academic publishers, 1998, pp. 331–344.
- [40] Umemura and Tomita, “Rapid Flame Propagation in a Vortex Tube in Perspective of Vortex Breakdown Phenomena.” *Combustion and Flame*, Vol. 125, 2001, pp. 820–838.

- [41] Kahler, C. J., Sammler, B., and Kompenhans, J., “Generation and control of tracer particles for optical flow investigations in air”, *Experiments in Fluids*, Vol. 33, 2002, pp. 736–742.
- [42] Melling, A., “Tracer particles and seeding for particle image velocimetry”, *Meas. Sci. Technol.*, Vol. 8, 1997, pp. 1406–1416.
- [43] Muruganandam Thiruchengode, “Sensing and dynamics of lean blowout in a swirl dump combustor”, PhD Dissertation, School of Aerospace Engineering, Georgia Institute of Technology, Atlanta, GA, May 2006.
- [44] Bradley D., Gaskell, P. H., Gu, X. J., Lawes, M., and Scott M. J., “Premixed turbulent flame instability and NO formation in lean-burn swirl burner”, *Combustion and Flame*, Vol. 115, 1998, pp. 515–538.
- [45] Satoru Ishizuka, “Flame propagation along a vortex axis”, *Progress in Energy and Combustion Science*, Vol. 28, 2002, pp. 477–542.